

Article

Effect of Turbulence Intensity on Aerodynamic Loads of Floating Wind Turbine under Wind–Wave Coupling Effect

Wenxin Tian^{1,2}, Qiang Shi³, Lidong Zhang³, Hehe Ren^{1,*}, Hongfa Yu¹, Yibing Chen³, Zhengcong Feng³ and Yuan Bai²

¹ Department of Airport and Civil Engineering, Nanjing University of Aeronautics and Astronautics, Nanjing 210016, China; twxtim@gmail.com (W.T.); yuhongfa@nuaa.edu.cn (H.Y.)

² State Key Laboratory of Low-Carbon Smart Coal-Fired Power Generation and Ultra-Clean Emission, China Energy Science and Technology Research Institute Co., Ltd., Nanjing 210023, China; baiyuan6049@163.com

³ School of Energy and Power Engineering, Northeast Electric Power University, 169 Changchun Road, Chuanying District, Jilin 132012, China; sq2093583214@163.com (Q.S.); nedu1015@aliyun.com (L.Z.); cyb04162022@163.com (Y.C.); fengzcc_neepu@163.com (Z.F.)

* Correspondence: renhehe@nuaa.edu.cn

Abstract: This study first employs TurbSim and OpenFAST (Fatigue, Aerodynamics, Structures, Turbulence) programs for secondary development to comprehensively model the NREL-5MW semi-submersible wind turbine and OC4-DeepC wind floating platform with wind–wave interaction. Next, we investigate the dynamic response of floating wind turbines under the complex coupling of turbulent winds and irregular waves. Turbulent wind fields were simulated using the IEC Kaimal model with turbulence intensities of 5% and 20%. Additionally, two irregular waves were simulated with the Pierson–Moskowitz (P–M) spectrum. The results indicate that in turbulent wind conditions, the aerodynamic power of the wind turbine and the root bending moments of the blades are significantly influenced by turbulence, while the impact of waves is minimal. The coupled motion response of the floating platform demonstrates that turbulence intensity has the greatest impact on the platform’s heave and pitch motions, underscoring the importance of turbulence in platform stability. This study provides essential insights for designing and optimizing floating wind turbines in complex wind–wave coupling offshore environments.

Keywords: floating wind turbine; turbulent wind; aerodynamic load; platform motion response



Citation: Tian, W.; Shi, Q.; Zhang, L.; Ren, H.; Yu, H.; Chen, Y.; Feng, Z.; Bai, Y. Effect of Turbulence Intensity on Aerodynamic Loads of Floating Wind Turbine under Wind–Wave Coupling Effect. *Sustainability* **2024**, *16*, 2967. <https://doi.org/10.3390/su16072967>

Academic Editors: Jerson Rogério Pinheiro Vaz, Wei Jun Zhu and Wenzhong Shen

Received: 25 February 2024

Revised: 27 March 2024

Accepted: 27 March 2024

Published: 2 April 2024



Copyright: © 2024 by the authors. Licensee MDPI, Basel, Switzerland. This article is an open access article distributed under the terms and conditions of the Creative Commons Attribution (CC BY) license (<https://creativecommons.org/licenses/by/4.0/>).

1. Introduction

With the development of the social economy and the depletion of traditional fossil energy, the use of renewable energy has become the focus of solving the energy problem, and wind energy, as a clean and renewable energy, has been increasingly emphasized by various countries because it is non-polluting, renewable, and has a large storage capacity [1,2]. Offshore wind power has grown in popularity in recent years, owing to its advantages of greater wind energy, distance from urban areas, and fewer limits [3]. According to the latest Global Wind Energy Report 2022 [4] released by the Global Wind Energy Council (GWEC), by the end of 2022, the total installed capacity of wind turbines in the world reached 906 million kilowatts, and the overall trend is toward clustering, large-scale, and oceanization. The increase in wind turbine capacity is accompanied by the development trend of lightweight and large-scale blade diameters. The typical slender structure of wind turbine blades inevitably leads to a more flexible blade structure. In the sea, under the action of complex incoming currents and platform movement, the blade will be subjected to more intense aerodynamic loads; the aerodynamic force, inertial force, and elastic force of the coupling effect will produce nonlinear deformation in the extreme working conditions and even cause damage and failure of the blade [5].

Offshore wind turbines are mainly divided into fixed and floating forms. Fixed structures are typically used in nearshore shallow waters, while floating wind turbines in waters deeper than 60 m exhibit better economic feasibility, reduced installation difficulty, and lower cost consumption [6]. The floating foundation of floating wind turbines is controlled by a mooring system hanging at sea, and its structure experiences nonlinear motion due to the combined impacts of wind and waves. In complex offshore environments, wind turbine blades may experience severe deformation or even accidents such as breakage under extreme conditions [7]. Therefore, in-depth research on the aerodynamic loads of floating wind turbines under the coupling of wind and waves is an urgent need.

Turbulence intensity is one of the important parameters to reveal the turbulence structure. Wind turbine loads are severely affected by the magnitude of the turbulence intensity of the incoming wind [8]. The biggest difference between a floating wind turbine and a stationary wind turbine is that a floating wind turbine is subjected to the coupling of wind and waves. Waves at sea cause complex multi-degree-of-freedom motions in floating wind turbines [9], resulting in uncontrollable changes in the interaction between the wind turbine blades and the incoming wind, and subjecting the wind turbine components to more intense loads and more complex fluctuations in aerodynamic performance.

Currently, scholars both domestically and internationally have conducted extensive research on the structural dynamic response of floating wind turbines under the coupling of wind and waves. Banerjee et al. [10], by studying a multi-degree-of-freedom model of offshore wind turbines, simulated random wind and wave loads using Von Karman turbulent wind spectra and P–M nonlinear wave spectra, respectively. They analyzed the structural wind–wave coupling and blade coupling effects, finding that under wind–wave coupling, the tower displacement is mainly controlled by wind loads, while acceleration and tower-top rotation are mainly controlled by wave loads. Velarde et al. [11] studied the fatigue reliability of a 10 MW offshore single-pile wind turbine under wind–wave coupling and pointed out the crucial influence of turbulence intensity on fatigue loads. They suggested that the minimum fatigue design factor (FDF) should be no less than three. Xu et al. [7], based on a newly developed nonlinear wave, conducted fatigue damage and critical response studies on floating wind turbines. They found that the fatigue loads on the tower base are mainly induced by waves, and the incoming wind is the primary factor affecting most of the turbine's motion.

Neeraj Aggarwal et al. [12] investigated the dynamic response characteristics of a floating wind turbine under harsh sea conditions by modeling the Spar platform floating wind turbine based on the potential flow theory and, using the hydrodynamic software Aqwa (2010), Jeon S H et al. [13] simulated the dynamic response of a Spar platform floating wind turbine under the action of turbulent wind and irregular waves, generating random waves using P–M wave spectra and employing a coupled iterative BEM–FEM method to analyze the interaction between the wave-floater structure and wave-mooring line.

However, the complexity of offshore wind and waves [14] makes the turbulence intensity of incoming wind crucial for the power and load distribution of floating wind turbines. Variations in turbulence intensity [15] can lead to abrupt changes in wind loads on various parts of the turbine structure, increasing fatigue loads, reducing safety, and shortening the lifespan [16–18]. Li et al. [19] used dynamic overflow computational fluid dynamics (CFD) and multi-body dynamics (MBD) for kinematic response calculations of aerodynamic loads and verified the validity of the turbulence model by comparing the expected statistics of the CFD-simulated turbulent wind field with the Mann-modeled turbulent inlet boundaries of the displayed wind. Marino et al. [16] compared linear and nonlinear wave models for a 5 MW wind turbine model under different wind and sea state modeling assumptions and pointed out that linear wave motion is the main cause of fatigue loading in wind turbines. Fu et al. [20] used a wind tunnel to collect wake data from a floating offshore wind turbine and discussed the effects of parameters such as pitch and sway vibration on the instantaneous power output and wake trajectory. Zheng et al. [21], using bidirectional fluid–structure coupling technology, numerically

simulated the NREL-5MW wind turbine and investigated the influence of turbulent wind with different intensities on the aerodynamic characteristics of the wind turbine.

Furthermore, the creation of turbulence prediction models not only helps to build wind turbine operation strategies, but it also serves as a reference for the construction of offshore floating wind turbines. XU et al. [22] based their turbulence prediction model on phase space reconstruction and a generalized learning system (BLS), which not only has higher prediction accuracy but also has a faster learning speed to meet the prediction requirements of the wind-wave coupling of floating wind turbines. Zhang et al. [23] propose an improved Dynamic Inverse Learning Jaya (DOLJaya) method, which is highly competitive and adaptable in terms of efficiency in solving complex nonlinear problems. Li et al. [24] propose a spatio-temporal prediction model based on the optimally weighted graphical convolutional network (GCN) and the gated recurrent unit (GRU), which takes full advantage of the spatio-temporal characteristics of the turbulence development to substantially improve the prediction accuracy. Xu et al. [25] found that by improving the Caputo–Fabrizio fractional order derivative SR in the vibration diagnosis of wind turbine systems, the weak vibration signals are amplified, which effectively improves the vibration detection efficiency of wind turbines operating in strong turbulence environments. Zhang et al. [26] proposed a new layout method for wind turbines. They studied the evolution process of wind turbine wake through the wind tunnel test, and analyzed the speed distribution and turbulence characteristics of wind farms through the turbulence intensity and other factors.

In conclusion, the effect of turbulence intensity on wind turbine loads and dynamic response is significant. Floating wind turbines frequently meet harsh sea conditions, making the wind-wave coupling effect an important research subject. It is worth emphasizing that there is currently a scarcity of in-depth studies on the effect of turbulence intensity on the aerodynamic loads of floating wind turbines under wind-wave coupling, both domestically and globally. As a result, this paper, using the OpenFAST version 3.0.0 (Fatigue, Aerodynamics, Structures, Turbulence) software, seeks to investigate the impact of wind-wave coupling at various turbulence intensities on the aerodynamic loads of the NREL-5MW semi-submersible wind turbine using simulation and modeling.

2. Research Object

The research focuses on the NREL-5MW wind turbine, and its main parameters are presented in Table 1. Additionally, the study utilizes the OC4-DeepCwind floating foundation, with its key parameters detailed in Table 2. Figure 1 shows the model of a 5 MW semi-submersible wind turbine.



Figure 1. Semi-submersible wind turbine.

Table 1. NREL-5MW Wind Turbine Parameters.

Parameter/Unit	Value
Rated power/MW	5
Number of blades/n	3
Hub height/m	90
Impeller diameter/m	126
Cut-in wind speed/(m·s ⁻¹)	3.0
Rated wind speed/(m·s ⁻¹)	11.4
Cutting wind speed/(m·s ⁻¹)	25.0

Table 2. Semi-submersible platform parameters.

Parameter/Unit	Value
Draft/m	22
Displacement/m ³	2.35 × 104
Platform mass/kg	2.17 × 107
Center of mass/m	−15.23
Roll inertia/(kg·m ²)	9.43 × 109
Pitch inertia/(kg·m ²)	9.43 × 109
Yaw inertia/(kg·m ²)	1.63 × 1010
Number of mooring lines n	3
Fairlead depth/m	9.5
Anchor depth/m	130
Distance to fairleads from platform centerline/m	44
Distance to anchors from platform centerline/m	691
Mooring line diameter/m	0.246
Mooring line mass/(kg·m ⁻¹)	375.38

3. Wave Coupling Loads

To comprehensively understand the performance of the NREL-5MW semi-submersible wind turbine under different turbulence intensities and sea conditions, numerical simulations were conducted to provide a diverse and comprehensive analysis of the impact on the aerodynamic characteristics of the floating wind turbine. Specifically, the inflow conditions of the wind turbine adopted the turbulence model of the IEC Kaimal wind spectrum, with normal wind as the turbulence type. Turbulence intensities were set at 5% and 20%. Additionally, irregular waves were simulated using the Pierson–Moskowitz (P–M) spectrum to generate two different wave spectra, with significant wave heights (H_s) set at 2.5 m and 5 m. The total simulation duration was 1000 s with a time step of 0.0125 s. This setup resulted in four different simulation scenarios, as detailed in Table 3.

Table 3. Environmental Condition.

Case	U (m/s)	I	H_s (m)	T_p (S)
1		5%	2.5	7.1
2		5%	5	10.3
3	11.4	20%	2.5	7.1
4		20%	5	10.3

These defined conditions allow for an in-depth investigation into the response of the NREL-5MW semi-submersible wind turbine under different turbulence and sea conditions, providing a more comprehensive understanding of the characteristics of its aerodynamic loads. This will contribute to a detailed and comprehensive data foundation for further analysis of the performance of floating wind turbines in complex offshore environments.

3.1. Environmental Wind Field

To simulate the inflow conditions of the wind turbine, Turbsim v2.0.0 software was employed to generate a turbulent wind field with a wind speed of 11.4 m/s. The turbulence model used the IEC Kaimal wind spectrum, and normal wind was selected as the turbulence type. Two different turbulence intensity levels were set at 5% and 20%. The specific simulation parameters are detailed in Table 4.

Table 4. Parameter values for turbulent wind farm simulation.

Simulation Parameters of Turbulent Wind Farm/Unit	Value
Turbulence spectrum model	IEC Kaimal
Two-dimensional wind farm grid node setup ($Y \times Z$)	31×31
Time step (s)	0.05
Effective simulation duration (s)	1000
Reference height (m)	90
Average wind speed at reference altitude/($\text{m}\cdot\text{s}^{-1}$)	11.4
IEC turbulence type	NTM
Mesh height Z (m)	160
Mesh width Y (m)	145
Turbulence intensity	5%, 20%

In this configuration, we considered the distribution of nodes in the two-dimensional wind farm grid and the average wind speed at the reference height. By selecting an appropriate time step, we could simulate the dynamic changes in the turbulent wind field over a relatively short duration. This setup provides robust support for in-depth research into the aerodynamic response of the wind turbine under different turbulence intensities. Under the combined action of various loads, considering the structural size of the wind turbine and its possible drift motion, the calculation domain of a wind field with a height of 160 m and a width of 145 m was selected and divided into a grid of 31×31 , as shown in Figure 2. Here, the turbulent wind generated by Turbsim circulates in a two-dimensional wind field. Incoming wind enters from the front entrance and exits in the x direction, thus circulating.

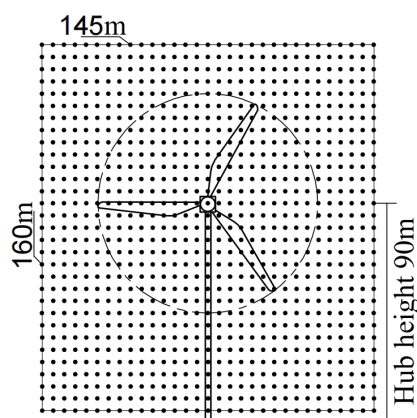


Figure 2. Wind field meshing.

3.2. Wind Loads

In this study, OpenFAST was utilized to calculate wind turbine loads, employing the classical blade element momentum theory. In this theory, the wind turbine blade is simplified into a finite number of blade elements. An iterative algorithm is employed to solve for the distribution of axial induction factor (a) and tangential induction factor (a') along the span of the blade. The finite element theory is combined with the blade element theory and momentum theory. Wind turbine blades are treated as finite segments. The lift and drag coefficients of the blade section airfoil are used to calculate the aerodynamic

forces acting on each blade element. Figure 3 shows the velocity triangles and forces acting on the airfoil. Where Ω is the rotor speed, r is the local radius of the blade element, V is the inflow velocity, W is the relative inflow velocity, a and b are the axial and tangential induction factors, α and β are, respectively, the effective angle of attack, torsion angle, and inflow angle of the blade element; ϕ is the relative inflow angle of the local element, and L and D are, respectively, the lift force and resistance generated by the blade element.

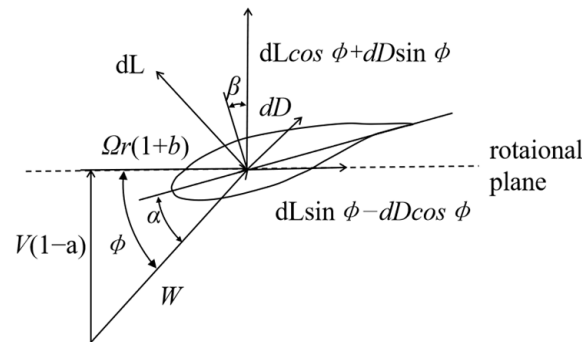


Figure 3. Illustration of the velocity triangle for a blade element.

The loads on each blade element are then integrated along the span. The aerodynamic loads on the wind turbine blade generated by the blade element momentum theory can be represented as the following:

$$dT = \frac{1}{2} \rho V^2 (C_L \cos \varnothing + C_D \sin \varnothing) c dr \quad (1)$$

$$dQ = \frac{1}{2} \rho V^2 (C_L \sin \varnothing - C_D \cos \varnothing) c dr \quad (2)$$

where T is the thrust force on the wind turbine rotor; Q is the torque; ρ is the actual air density; V is the relative inflow wind speed at the rotor; C_L and C_D are the lift and drag coefficients, respectively; \varnothing is the angle of attack; c is the chord length of a blade element; and r is the radial distance from the blade to the hub.

The turbulent wind at the hub height is characterized by wind speeds in three directions: along the wind direction (axial), perpendicular to the wind direction (transverse), and vertically. Turbulence intensity is defined as the ratio of the standard deviation of the wind speed (root mean square of the fluctuating wind speed) to the average wind speed, the formula is as follows:

$$I = \frac{\sqrt{u'^2 + v'^2 + w'^2}}{\sqrt{\overline{u^2} + \overline{v^2} + \overline{w^2}}} = \frac{\sqrt{u'^2 + v'^2 + w'^2}}{\overline{V}} \quad (3)$$

where u , v , and w are velocity components in vertical, horizontal, and vertical orthogonal directions, respectively. And w' are the three components of fluctuating wind speed, respectively. Figure 4 illustrates the wind speed distribution at the hub height under two different turbulence intensities.

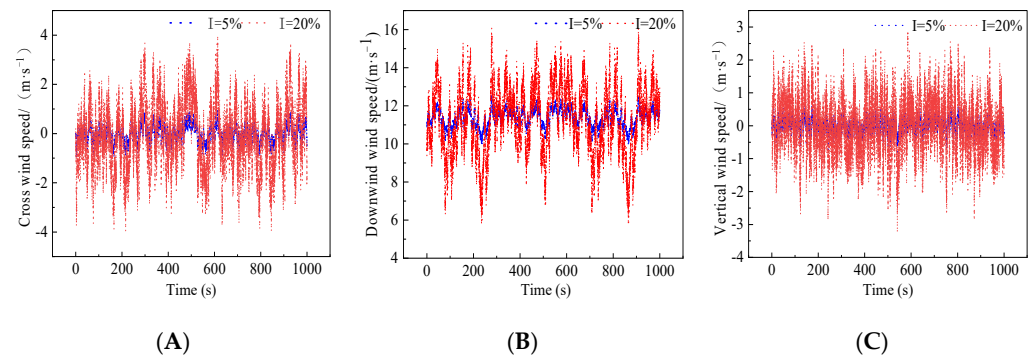


Figure 4. Wind speed of two turbulence intensities at wheel hub height. (A–C) represent u , v , and w , respectively.

3.3. Wave Loads

When offshore floating wind turbines operate at sea, they experience the complex coupling of turbulent winds and waves, resulting in multi-degree-of-freedom complex motions. Many researchers commonly employ wave spectra to study wave loads. After dimensionless analysis of the average spectrum obtained by different wind speed groups, Pierson et al. [27] obtained each quantity in the dimensional spectrum by fitting; a complete wave spectrum model was obtained, that is, a Pierson–Moskowitz spectrum (also known as P–M spectrum). The P–M spectrum is applicable to the sea surface in a fully extended state, and wind speed is its only variable parameter.

In this study, the P–M spectrum is chosen to simulate irregular waves, with significant wave heights of 2.5 m and 5 m and spectral peak periods of 7.1 s and 10.3 s. Wave height is defined by actual measured ocean data over the eastern United States [28]. The expressions for the P–M spectrum are given by:

$$SPM = \frac{4 \cdot H_s^2}{\pi^2} \cdot \omega^5 \cdot \exp\left(-\frac{5 \cdot \omega^4}{4 \cdot \omega_p^4}\right) \quad (4)$$

where SPM provides the energy contributed by each component wave in different frequency intervals, H_s is the significant wave height, ω_p is the spectral peak frequency, and ω is the wave circular frequency. Figure 5 shows two different kinds of waves.

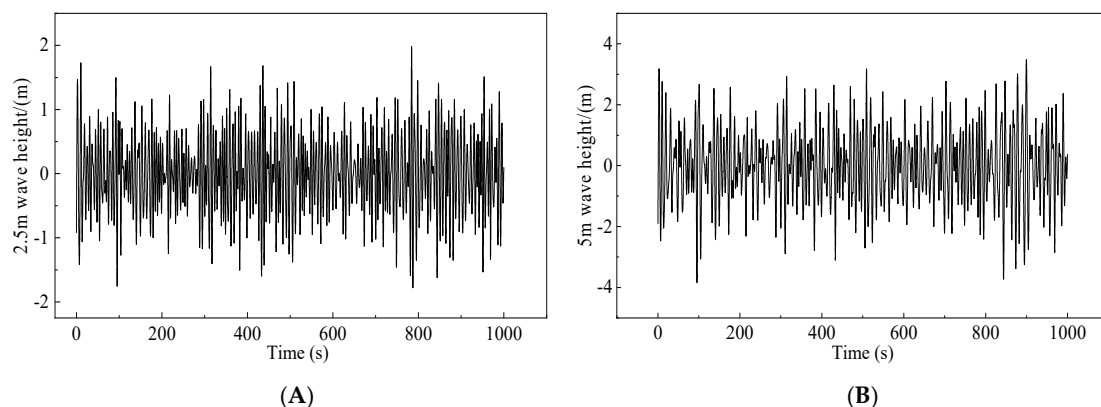


Figure 5. Two kinds of irregular waves. (A) shows irregular waves with a significant wave height of 2.5 m and a spectral peak period of 7.1 s, while (B) displays irregular waves with a significant wave height of 5 m and a spectral peak period of 10.3 s.

Due to the large size of the semi-submersible platform in this study, its response to waves cannot be ignored. Therefore, the radiation/diffraction theory is employed to

calculate wave loads. Assuming the seawater is an incompressible, irrotational, and inviscid ideal fluid, the total velocity potential Φ in the flow field can be expressed as the following:

$$\Phi = \Phi_I + \Phi_D + \Phi_R \quad (5)$$

$$\frac{\partial \Phi}{\partial t} + g\eta = p\omega + \frac{1}{2}\rho_w \left(\frac{\partial \Phi}{\partial s} \right)^2 \quad (6)$$

where Φ_I is the incident potential, Φ_D is the diffracted potential, and Φ_R is the radiated potential. The total velocity potential in the wave field satisfies the Laplace equation and the corresponding boundary conditions. Specifically, for the free surface boundary condition, it can be expressed as the following:

$$\left\{ \begin{array}{l} \partial^2 \Phi / \partial x^2 + \partial^2 \Phi / \partial y^2 + \partial^2 \Phi / \partial z^2 = 0 \\ \partial \Phi / \partial s = \partial \eta / \partial t + (\partial \eta / \partial x) \cdot (\partial \Phi / \partial x) + (\partial \eta / \partial y) \cdot (\partial \Phi / \partial y) \\ \partial \Phi / \partial t = 0.5(\nabla \Phi)^2 + P_w / \rho_w + gs = 0 \\ \partial \Phi / \partial z|_{z=h} = 0 \\ \partial \Phi / \partial \vec{n} = 0 \end{array} \right. \quad (7)$$

where g is the acceleration due to gravity, t is time, h is the water depth, P_w is the pressure at the water surface, \vec{n} is the outward normal direction vector to the wet surface, η is the free surface elevation, ρ_w is the water density, and s is the free surface. This method of solving wave loads will serve as a foundation for analyzing the dynamic response of floating wind turbines under different wave conditions.

The hydrodynamic pressure F_d on the surface of the floating body can be obtained by the Bernoulli equation, and the wave load F_W , wave moment, and wave vector M_W can be obtained by solving the equation.

$$F_d = -\partial \Phi / \partial t \quad (8)$$

$$F_W = \iint_{S_B} S_B - P_w \vec{n} dS_B \quad (9)$$

$$M_W = \iint_{S_B} S_B - F_d \vec{r} \times \vec{n} dS_B \quad (10)$$

where S_B is the wet surface of the platform and \vec{r} the tangent vector of the platform surface.

4. Simulation Validation

To validate the reliability of the turbulent wind model generated by Turbsim, this study conducted a frequency spectrum analysis on simulated wind data with a 5% turbulence intensity. The data was transformed into a power density spectrum and compared with the theoretical formula of the IEC Kaimal wind spectrum. Taking longitudinal wind speed as an example, the theoretical power density spectrum formula for longitudinal wind speed in the Kaimal model is given by the following:

$$S(f) = \frac{4 \cdot \sigma^2 \cdot L}{\pi \cdot V_{\text{hub}}} \cdot \frac{1}{(1 + 4 \cdot f \cdot L / V_{\text{hub}})^{5/3}} \quad (11)$$

where f is the frequency, S is the power density, σ is the velocity standard deviation, L is the turbulence integral scale, and hub V_{hub} is the hub height wind speed at 90 m.

From Figure 6A, it can be observed that the simulated power spectrum of longitudinal wind speed aligns well with the frequency domain variations of the IEC Kaimal target function spectrum. Therefore, it can be concluded that the turbulent fluctuating wind field established in this study is reasonably reliable.

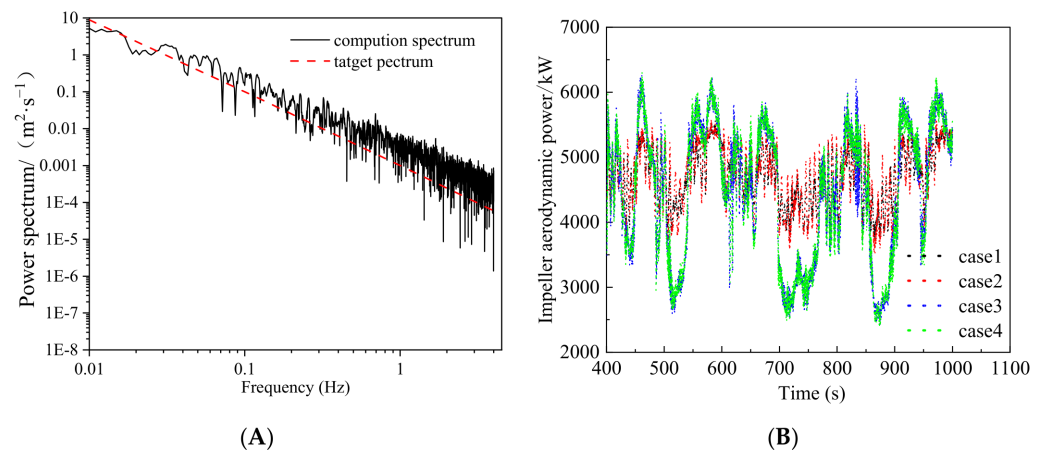


Figure 6. (A) Longitudinal wind speed power spectrum vs. Kaimal and (B) aerodynamic load of wind turbine impeller.

These validation results indicate that the turbulent wind model used in this study aligns with theoretical formulas in the frequency domain, ensuring accurate simulation of the dynamic response of floating wind turbines under different turbulence conditions.

The NREL-5MW wind turbine selected in this paper is controlled by variable speed and variable pitch. According to the literature [29], the generator and rotor speeds of 5 MW wind turbines increase linearly with wind speed to maintain a constant blade tip speed ratio and optimal wind power conversion efficiency. Similarly, generator and rotor power and generator and rotor torque also increase sharply with the increase in wind speed, showing three times and two times, respectively. Above the rated power, the generator and rotor power are kept constant by adjusting to a fixed speed through active pitch control.

In order to verify the authenticity of the output results in this paper, the power speed curve given by the official NREL-5MW wind turbine [30] was compared. The result is shown in Figure 7. As can be seen from the figure, the results of this paper are highly consistent with the official results, indicating the feasibility and authenticity of the output results of this paper.

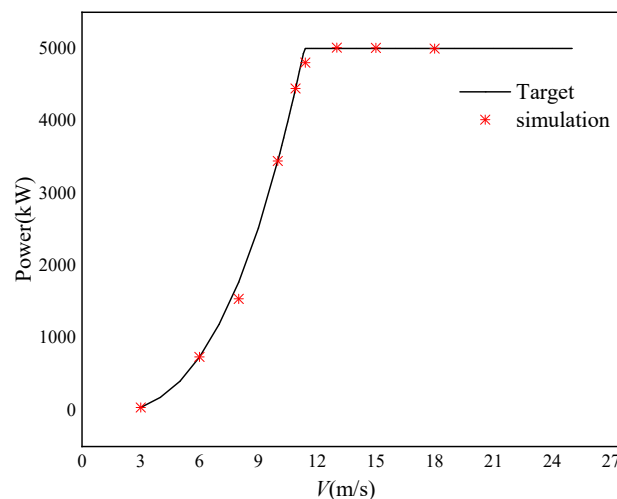


Figure 7. Power curve comparison.

5. Results and Analysis

To analyze the impact of turbulence intensity in inflow wind and waves on the aerodynamic loads of floating wind turbines, we selected an inflow wind with a rated speed of 11.4 m/s and considered two different turbulence intensities: 5% and 20%. Additionally, we used the P-M spectrum to simulate two types of irregular waves as input conditions.

A fully coupled simulation of the NREL-5MW semi-submersible wind turbine was conducted using OpenFAST 3.0.0 software, with a simulation duration of 1000 s. To ensure the accuracy of the simulation results, unstable data from the first 400 s were excluded.

In this setup, we focus on the aerodynamic load responses of the floating wind turbine under different turbulence and wave conditions, as well as potential structural dynamic responses. The results of the fully coupled simulation provide in-depth insights into the complex dynamic characteristics of floating wind turbines during offshore operation, offering a robust reference for design and optimization.

5.1. Analysis of Generating Power and Blade Root Bending Moment

From Figure 4B, it can be observed that in underrated wind speed conditions, the aerodynamic power of the wind turbine fluctuates significantly with an increase in turbulence intensity in the inflow wind. The larger the turbulence intensity, the more pronounced the fluctuation. In contrast, the variation in wave height has a relatively small impact on the aerodynamic power of the wind turbine. Additionally, by comparing Figures 2 and 4B, it is evident that the trend of aerodynamic power changes in sync with the variation in inflow wind at the hub height, exhibiting a high correlation.

In the same sea conditions, when the turbulence intensity in the inflow wind increases from 5% to 20%, the standard deviation of the wind turbine's aerodynamic power increases by 121.62% and 98.88%, respectively. However, under the same turbulence intensity, when the significant wave height increases from 2.5 m to 5 m, the aerodynamic power of the wind turbine increases by 13.64% and 1.35%, respectively. The overall results indicate that the aerodynamic power of the wind turbine is primarily influenced by wind loads, while wave loads have a minor impact. This is attributed to the influence of mooring cables on the foundation of the floating wind turbine, leading to a significant effect of wave loads on the motion response of the floating foundation, with little effect on the wind turbine blades. Conversely, the turbulence intensity in the inflow wind, representing the relative strength of turbulent wind speed, directly affects the fluctuation of wind loads, resulting in noticeable amplitude fluctuations in aerodynamic power.

Figure 6B shows the fluctuation of the wind turbine's aerodynamic power. Figure 8A, Figure 8B, and Figure 8C respectively show the swinging moment, flapping moment, and torsional moment at the blade root of the wind turbine over time. These moments exhibit periodic changes over time, with an increase in turbulence intensity causing significant variations in the blade root moments. It is noteworthy that the swinging moment is primarily caused by the weight of the wind turbine blade itself, resulting in a relatively smaller correlation with turbulence intensity and sea conditions. The standard deviation of the flapping moment experiences a significant increase, indicating that turbulence intensity has the most significant impact on the flapping moment at the blade root. The time series of the flapping moment shows continuous variation over time, presenting a large cycle with a duration of 100 s, featuring low points and high points at semi-cycles.

Table 5 provides statistical characteristics of the changes in wind turbine output power and aerodynamic loads during the 1000 s. As the turbulence intensity in the inflow wind increases, the standard deviations of the swinging, flapping, and torsion moments at the blade root also increase accordingly. Particularly, the standard deviation of the flapping moment experiences a substantial increase, indicating that turbulence intensity has the most significant impact on the flapping moment at the blade root. The changes in power output and aerodynamic loads of the wind turbine under different turbulence intensities and wave conditions exhibit complex correlations in trends and amplitude changes. This is significant for further understanding the dynamic response characteristics of floating wind turbines.

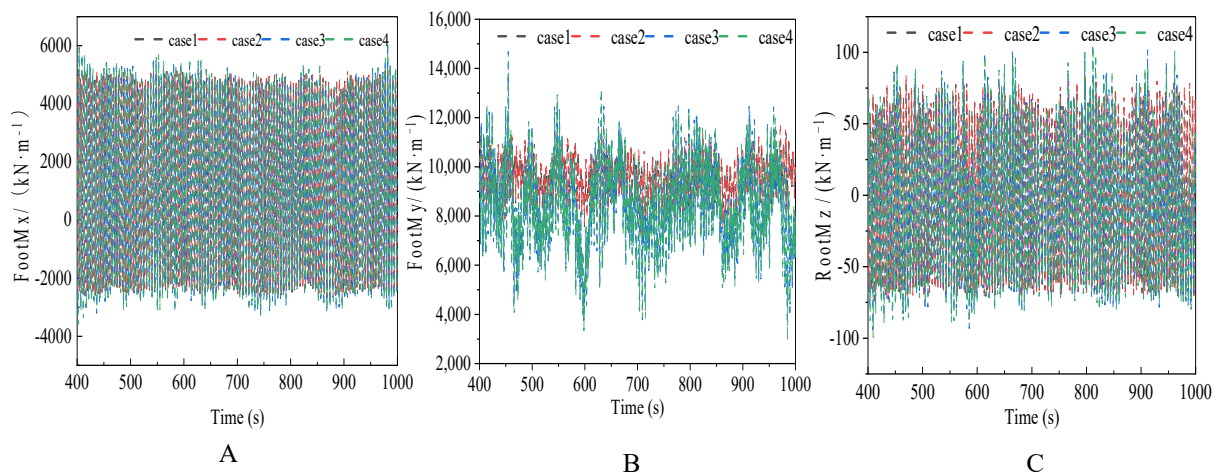


Figure 8. (A) Swinging moment of blade root, (B) flapping moment of blade root, and (C) torsion moment of blade root.

Table 5. NREL-5MW Wind Turbine 1000 s hour output power and aerodynamic loads.

Data Characteristics	Condition	Power (kW)	FootMx (kN/m)	FootMy (kN/m)	FootMz (kN/m)
Standard deviation	1	463.08	2563.21	696.43	45.31
	2	522.98	2563.67	763.35	45.39
	3	1026.30	2587.06	1527.35	42.11
	4	1040.12	2585.94	1555.62	42.11
Maximum value	1	5557.89	5304.04	11,501.70	83.75
	2	5480.24	5290.85	11,752.30	85.08
	3	5901.14	6061.52	14,667.85	105.91
	4	5704.84	5999.14	14,228.04	103.99
Mean value	1	4679.64	1198.59	9582.22	2.25
	2	4686.84	1199.72	9575.68	2.24
	3	4412.35	1139.37	8460.51	−3.16
	4	4416.26	1141.27	8452.50	−3.19
Minimum value	1	58.92	−3163.23	264.66	−75.64
	2	58.89	−3259.60	264.10	−73.86
	3	58.77	−3357.63	279.77	−94.21
	4	58.73	−3580.81	279.21	−99.30

5.2. Analysis of Platform Coupled Motion Response

Figure 9 presents the time-domain responses of the semi-submersible platform under different operating conditions, with both wind and waves propagating along the positive X-axis. The simulation duration is 1000 s, with the initial 400 s discarded to eliminate the transient effects of wind turbine startup on the system's dynamic response. The examination of the six-degrees-of-freedom motion reveals that, among various motions, the platform's responses in surge, sway, and heave are most prominently affected.

The surge motion of the platform, depicted in Figure 9A and summarized in Table 6, exhibits notable standard deviations under varying turbulence intensities and sea states. As turbulence intensity and wave height increase, the standard deviation of surge also rises, indicating a reduction in platform stability. Specifically, under a turbulence intensity of 5%, the standard deviation of surge increases by 25% as the wave height transitions from 2.5 m to 5 m. This trend is more pronounced with a turbulence intensity of 20%, showing a 4.3% increase in the standard deviation of surge under the same wave height conditions.

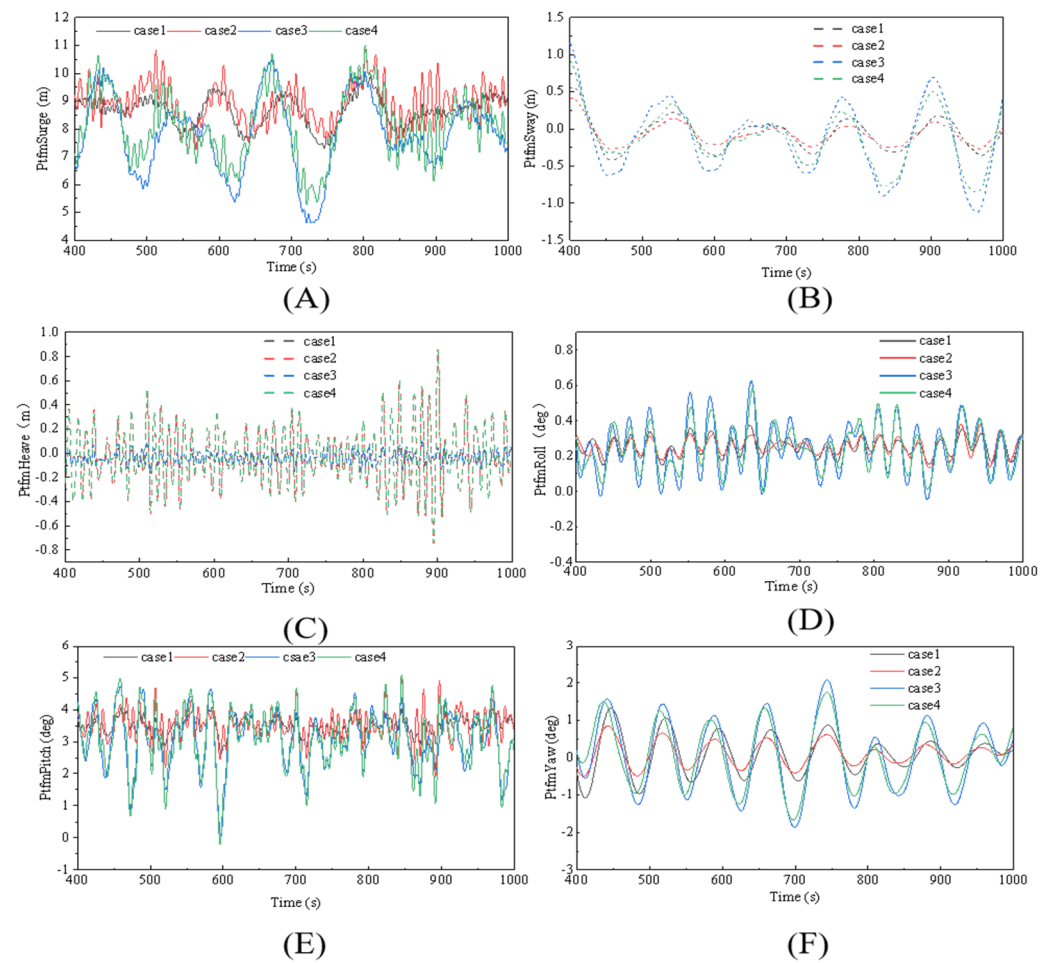


Figure 9. Time domain motion response of platform. (A–F) is the six degrees of freedom movement of the platform, namely surge, sway, heave, roll, pitch and yaw.

Table 6. Platform motion response statistics table.

Data Characteristics	Case	Surge (m)	Sway (m)	Heave (m)	Roll (°)	Pitch (°)	Yaw (°)
Standard deviation	1	0.54	0.21	0.04	0.05	0.25	0.52
	2	0.71	0.14	0.23	0.05	0.45	0.31
	3	1.36	0.47	0.05	0.14	0.86	0.95
	4	1.20	0.35	0.24	0.12	0.90	0.82
Maximum value	1	9.95	0.07	−0.05	0.27	3.52	0.13
	2	10.86	−0.03	0.01	0.30	3.37	0.16
	3	10.58	0.07	−0.09	0.20	4.11	0.61
	4	11.02	−0.15	0.02	0.44	3.50	0.15
Mean value	1	8.64	−0.07	−0.04	0.25	3.51	0.09
	2	8.92	−0.08	−0.03	0.25	3.52	0.10
	3	7.82	−0.14	−0.03	0.24	3.07	0.04
	4	8.12	−0.13	−0.02	0.24	3.09	0.05
Minimum value	1	7.14	0.45	−0.03	0.30	3.03	0.51
	2	6.99	−0.24	0.25	0.19	4.49	−0.13
	3	4.62	−0.57	−0.03	0.16	2.92	0.11
	4	5.28	−0.46	−0.11	0.19	3.10	0.25

Similar to the surge, the sway motion of the platform experiences increased standard deviations with escalating turbulence intensity and wave height, as illustrated in Figure 9B

and corroborated by Table 6. The standard deviation of sway is particularly sensitive to turbulence intensity, demonstrating a 37% increase when transitioning from a turbulence intensity of 5% to 20% under a 5 m wave scenario. This underscores the heightened influence of turbulence intensity on the sway motion of the floating platform.

Contrary to surge and sway, the heave motion of the platform displays a comparatively smaller sensitivity to turbulence intensity. Wave effects are more prominent in influencing heave, as evidenced by Figure 9C and the statistics in Table 6. A detailed comparison between case sets reveals that, as turbulence intensity increases from 5% to 20%, the standard deviation of heave experiences a modest 4.3% rise under similar sea conditions.

The rotational motions of the platform, including roll, pitch, and yaw, are also influenced by turbulence intensity and wave height, as depicted in Figure 9D, Figure 9E, and Figure 9F, respectively. These rotational motions exhibit increased standard deviations under elevated turbulence intensity, indicating the diminishing stability of the platform.

The statistical overview provided in Table 6 encapsulates the standard deviation, maximum, mean, and minimum values for each degree of freedom motion under different environmental conditions. Notably, the surge and sway motions demonstrate a substantial increase in standard deviation with heightened turbulence intensity and wave height, signifying a pronounced impact on platform stability. Conversely, heave, being less responsive to turbulence intensity, is primarily influenced by wave effects.

These comprehensive analyses of platform motion responses under varying turbulence and wave conditions contribute to a more nuanced understanding of the intricate dynamics involved in the operation of floating wind turbines. The findings offer crucial insights for optimizing design parameters and enhancing the overall performance and stability of such systems in challenging marine environments.

5.3. Analysis of Velocity in Wake Region

The wake model in the AeroDyn module adopts the blade element momentum theory to conduct a dynamic simulation of wind turbine characteristics in time and region. The blades are divided into wirelessly thin blade units along the radius direction. When the load borne by the blades suddenly changes, the wake will quickly change accordingly. In the Wake Dynamics module, advection, deflection, and meandering models of wake are used to describe the propagation and diffusion process of the wake generated by the wind turbine in space. The wake is transported by turbulent vortices of different scales, and large-scale turbulent vortices directly affect the wind turbine wake meandering. Small-scale turbulent vortices affect the loss evolution of the wind turbine wake [30].

Figure 10 illustrates the wake velocity distributions under four distinct operating conditions at 1000 s. From Figure 10A,B, it can be observed that, despite variations in wave height and period, the velocity patterns are generally similar, suggesting a relatively minor influence of waves on the wake region. As turbulence intensity increases, it tends to reduce the area of low-velocity regions in the wake to some extent, resulting in a faster recovery of wake velocity.

To analyze the wake variation patterns, statistical data were collected for the wind turbine positions and average axial velocities at downstream locations of 3D, 5D, and 7D. The changes in axial velocities with height at different wake positions are illustrated in Figure 11. Under various operational conditions, distinct velocity variations are observed within the wind turbine rotor area. At a 5% turbulence intensity, notable velocity fluctuations are observed near the lower blade tip position, resulting in velocity deficits at the blade tip and hub center height. Beyond 5D, the velocity begins to recover. With an increase in turbulence intensity, the impact of the wind turbine on velocities at different heights gradually diminishes.

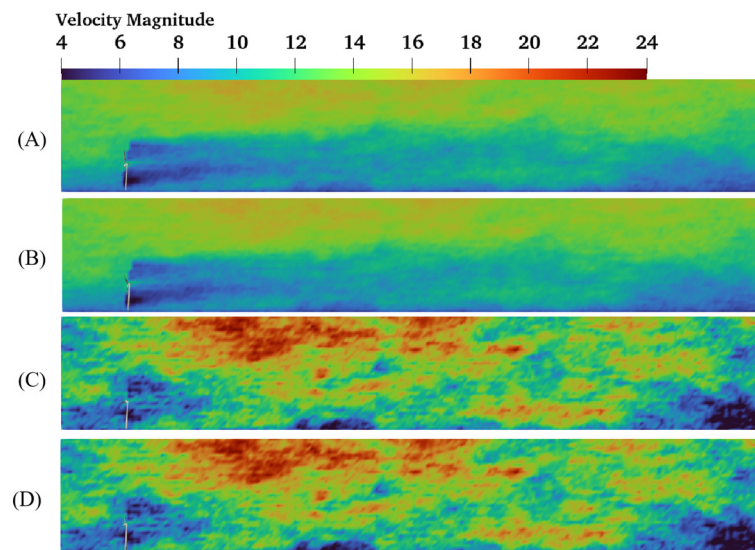


Figure 10. Wake velocity cloud image. (A–D) reveals that different turbulence intensities impact wake velocity.

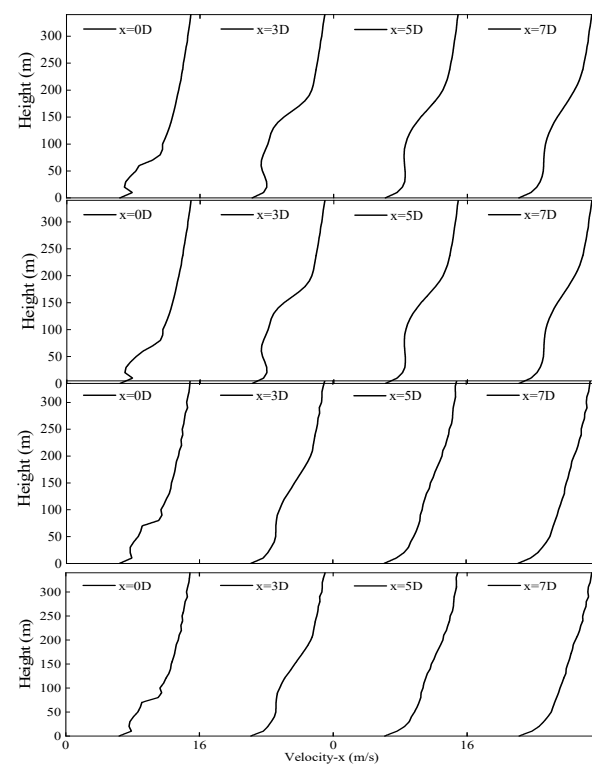


Figure 11. Velocity distribution of different flow directions.

Figure 12 depicts the distribution of velocity deficits in the x-y plane at the hub height downstream of the wind turbine. As the downstream distance increases, the velocity gradually recovers. From Figure 12A,B, it is evident that at $x = 3D$, $5D$, and $7D$, the velocity deficits at the wake center are 0.3, 0.25, and 0.17, respectively. Similarly, from Figure 9C,D, the velocity deficits are 0.16, 0.05, and 0.02. Comparing Figure 9A,B with Figure 9C,D, it can be observed that under different turbulence intensities, the trend of velocity deficit changes at the hub height remains consistent. With an increase in downstream position, the velocity deficit initially increases and then decreases.

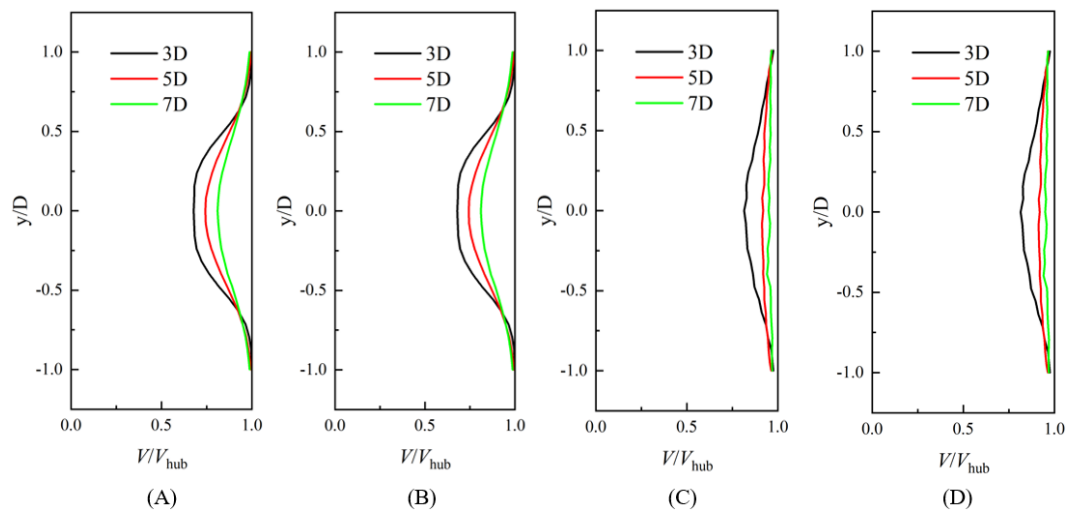


Figure 12. Loss of spanwise wake velocity. (A–D) corresponds to the speed loss under case1-case4 conditions respectively.

The influence of turbulence intensity on wake velocity deficit is more pronounced in the near-wake region. As turbulence intensity increases, the velocity deficit at different positions on the hub center plane in the x - y plane becomes smaller, resulting in a quicker recovery of velocity.

6. Conclusions

In this study, a complete examination of the dynamic response of the NREL-5MW semi-submersible wind turbine to turbulent winds and varied sea conditions was conducted using the secondary development of OpenFAST 3.0.0 and Turbsim v2.0.0. Furthermore, the study investigates and scrutinizes the six-degrees-of-freedom motion of the OC4-DeepCwind floating foundation in a variety of maritime conditions. Some insights gained from this research can be concisely described as follows:

- (1) **Aerodynamic Performance Dominance:** Wind-induced loads dominate the wind turbine's aerodynamic power output, with wave-induced loads having just a minor contribution. Power oscillations in response to increased turbulence intensity are notable for their size and turbulent character. Surprisingly, fluctuations in wave height have little effect on the aerodynamic performance of the wind turbine.
- (2) **Root Bending Moment Sensitivity:** Root bending moment loads at the blade root of the wind turbine predominantly originate from wind-induced loads, displaying limited sensitivity to wave effects. As turbulence intensity escalates, there is a discernible intensification of loads at the blade root. Specifically, the standard deviation of the flap, lead-lag, and torsional moments at the blade root increases proportionally, with the lead-lag moment exhibiting the most pronounced surge. This underscores the predominant impact of turbulence intensity on the lead-lag moment at the blade root.
- (3) **Platform Coupled Motion Response:** Examining the platform's six-degrees-of-freedom motion, it is evident that turbulent winds and waves exert the most significant influence on surge, sway, and heave. Turbulence intensity, particularly in wind flows, appears as the most important driver of the floating wind turbine platform's dynamic response. As turbulence strength and wave height increase, platform stability decreases.
- (4) **Performance under Combined Environmental Factors:** When turbulence intensity is set at 5%, the floating platform exhibits increased sway under wave conditions transitioning from a 2.5 m to a 5 m wave height scenario, with a 37% increase in maximum amplitude and a 30% growth in standard deviation. In contrast, at 20% turbulence intensity, the platform's sway amplitude and standard deviation decrease. This shows

that the platform's longitudinal displacement is minimized, and its stability improves when high turbulence intensity and large wave scenarios are coupled.

- (5) Wind Turbine Wave Effect: Wave height and period have a minimal impact on wake velocity, while turbulence intensity exerts a more substantial influence. There are noticeable variations in wind speed within the wind turbine rotor area. As turbulence intensity increases, the velocity deficit at the hub center decreases, resulting in a faster recovery of velocity.

Author Contributions: W.T.: Methodology, writing—review and editing. Q.S.: Data curation, writing—original draft. L.Z.: Methodology, supervision, writing—original draft. H.R.: Supervision, writing—review and editing. H.Y.: Writing—original draft, resources. Y.C.: Writing—original draft. Z.F.: Writing—original draft, methodology, and investigation. Y.B.: Writing—original draft, software. All authors have read and agreed to the published version of the manuscript.

Funding: This research was funded by the Key R&D projects of Jilin Provincial Science (20200403141SF); Study on nonlinear wind robustness of structural systems for large-scale wind power generation (D2022FK101); the National Natural Science Foundation of China (52078251) and the National key r&d program (2019YFB1503701).

Data Availability Statement: The data that support the findings of this study are available from the corresponding author upon reasonable request.

Acknowledgments: The authors extend their profound gratitude to the State Key Laboratory of Low-carbon Smart Coal-fired Power Generation and Ultra-clean Emission. Their expertise and support in the development and maintenance of this essential tool have greatly facilitated our research.

Conflicts of Interest: Authors Wenxin Tian and Yuan Bai were employed by the company China Energy Science and Technology Research Institute Co., Ltd. The remaining authors declare that the research was conducted in the absence of any commercial or financial relationships that could be construed as a potential conflict of interest.

References

1. Wang, B.; Xu, Z.; Li, C.; Wang, D.; Ding, Q. Hydrodynamic characteristics of forced oscillation of heave plate with fractal characteristics based on floating wind turbine platform. *Ocean Eng.* **2020**, *212*, 107621. [CrossRef]
2. Yang, Y.; Bashir, M.; Li, C.; Wang, J. Analysis of seismic behaviour of an offshore wind turbine with a flexible foundation. *Ocean Eng.* **2019**, *178*, 215–228. [CrossRef]
3. Musial, W.; Spitsen, P.; Beiter, P.; Duffy, P.; Marquis, M.; Cooperman, A.; Rob, H.; Melinda, M.; Jennifer, K.; Sriharan, S. *Offshore Wind Market Report: 2021 Edition*; National Renewable Energy Laboratory (NREL): Golden, CO, USA, 2021. [CrossRef]
4. GWEC-GLOBAL-WIND-REPORT-2022 n.d. Available online: <https://gwec.net/wp-content/uploads/2022/03/GWEC-GLOBAL-WIND-REPORT-2022.pdf> (accessed on 24 February 2024).
5. Huo, F.; Zhao, Y.; Zhang, J.; Zhang, M.; Yuan, Z.-M. Study on wave slamming characteristics of a typical floating wind turbine under freak waves. *Ocean Eng.* **2023**, *269*, 113464. [CrossRef]
6. Lin, L.; Wang, K.; Vassalos, D. Detecting wake performance of floating offshore wind turbine. *Ocean Eng.* **2018**, *156*, 263–276. [CrossRef]
7. Xu, K.; Zhang, M.; Shao, Y.; Gao, Z.; Moan, T. Effect of wave nonlinearity on fatigue damage and extreme responses of a semi-submersible floating wind turbine. *Appl. Ocean Res.* **2019**, *91*, 101879. [CrossRef]
8. Yao, T.; Lu, Q.; Wang, Y.; Zhang, Y.; Kuang, L.; Zhang, Z.; Zhao, Y.; Han, Z.; Shao, Y. Numerical investigation of wake-induced lifetime fatigue load of two floating wind turbines in tandem with different spacings. *Ocean Eng.* **2023**, *285*, 115464. [CrossRef]
9. Antonutti, R.; Peyrard, C.; Johanning, L.; Incecik, A.; Ingram, D. The effects of wind-induced inclination on the dynamics of semi-submersible floating wind turbines in the time domain. *Renew. Energy* **2016**, *88*, 83–94. [CrossRef]
10. Banerjee, A.; Chakraborty, T.; Matsagar, V.; Achmus, M. Dynamic analysis of an offshore wind turbine under random wind and wave excitation with soil-structure interaction and blade tower coupling. *Soil Dyn. Earthq. Eng.* **2019**, *125*, 105699. [CrossRef]
11. Velarde, J.; Kramhøft, C.; Sørensen, J.D.; Zorzi, G. Fatigue reliability of large monopiles for offshore wind turbines. *Int. J. Fatigue* **2020**, *134*, 105487. [CrossRef]
12. Aggarwal, N.; Manikandan, R.; Saha, N. Nonlinear short term extreme response of spar type floating offshore wind turbines. *Ocean Eng.* **2017**, *130*, 199–209. [CrossRef]
13. Jeon, S.H.; Cho, Y.U.; Seo, M.W.; Cho, J.R.; Jeong, W.B. Dynamic response of floating substructure of spar-type offshore wind turbine with catenary mooring cables. *Ocean Eng.* **2013**, *72*, 356–364. [CrossRef]
14. Shi, W.; Liu, Y.; Wang, W.; Cui, L.; Li, X. Numerical study of an ice-offshore wind turbine structure interaction with the pile-soil interaction under stochastic wind loads. *Ocean Eng.* **2023**, *273*, 113984. [CrossRef]

15. Tian, W.; Tie, H.; Ke, S.; Wan, J.; Zhao, X.; Zhao, Y.; Zhang, L.; Wang, S. Numerical Investigation of the Influence of the Wake of Wind Turbines with Different Scales Based on OpenFOAM. *Appl. Sci.* **2022**, *12*, 9624. [\[CrossRef\]](#)
16. Marino, E.; Giusti, A.; Manuel, L. Offshore wind turbine fatigue loads: The influence of alternative wave modeling for different turbulent and mean winds. *Renew. Energy* **2017**, *102*, 157–169. [\[CrossRef\]](#)
17. Li, L.; Liu, Y.; Yuan, Z.; Gao, Y. Wind field effect on the power generation and aerodynamic performance of offshore floating wind turbines. *Energy* **2018**, *157*, 379–390. [\[CrossRef\]](#)
18. Kim, D.-Y.; Kim, Y.-H.; Kim, B.-S. Changes in wind turbine power characteristics and annual energy production due to atmospheric stability, turbulence intensity, and wind shear. *Energy* **2021**, *214*, 119051. [\[CrossRef\]](#)
19. Li, Y.; Castro, A.M.; Sinokrot, T.; Prescott, W.; Carrica, P.M. Coupled multi-body dynamics and CFD for wind turbine simulation including explicit wind turbulence. *Renew. Energy* **2015**, *76*, 338–361. [\[CrossRef\]](#)
20. Fu, S.; Jin, Y.; Zheng, Y.; Chamorro, L.P. Wake and power fluctuations of a model wind turbine subjected to pitch and roll oscillations. *Appl. Energy* **2019**, *253*, 113605. [\[CrossRef\]](#)
21. Zheng, X.; Yao, Y.; Hu, Z.; Yu, Z.; Hu, S. Influence of Turbulence Intensity on the Aerodynamic Performance of Wind Turbines Based on the Fluid-Structure Coupling Method. *Appl. Sci.* **2022**, *13*, 250. [\[CrossRef\]](#)
22. Xu, X.; Hu, S.; Shi, P.; Shao, H.; Li, R.; Li, Z. Natural phase space reconstruction-based broad learning system for short-term wind speed prediction: Case studies of an offshore wind farm. *Energy* **2023**, *262*, 125342. [\[CrossRef\]](#)
23. Zhang, L.; Hu, T.; Zhang, L.; Yang, Z.; McLoone, S.; Menhas, M.I.; Guo, Y. A novel dynamic opposite learning enhanced Jaya optimization method for high efficiency plate–fin heat exchanger design optimization. *Eng. Appl. Artif. Intell.* **2023**, *119*, 105778. [\[CrossRef\]](#)
24. Xu, X.; Hu, S.; Shao, H.; Shi, P.; Li, R.; Li, D. A spatio-temporal forecasting model using optimally weighted graph convolutional network and gated recurrent unit for wind speed of different sites distributed in an offshore wind farm. *Energy* **2023**, *284*, 128565. [\[CrossRef\]](#)
25. Xu, X.; Li, B.; Qiao, Z.; Shi, P.; Shao, H.; Li, R. Caputo-Fabrizio fractional order derivative stochastic resonance enhanced by ADOF and its application in fault diagnosis of wind turbine drivetrain. *Renew. Energy* **2023**, *219*, 119398. [\[CrossRef\]](#)
26. Zhang, L.; Feng, Z.; Zhao, Y.; Xu, X.; Feng, J.; Ren, H.; Zhang, B.; Tian, W. Experimental Study of Wake Evolution under Vertical Staggered Arrangement of Wind Turbines of Different Sizes. *J. Mar. Sci. Eng.* **2024**, *12*, 434. [\[CrossRef\]](#)
27. Pierson, W.J.; Moskowitz, L. A proposed spectral form for fully developed wind seas based on the similarity theory of S. A. Kitaigorodskii. *J. Geophys. Res.* **1964**, *69*, 5181–5190. [\[CrossRef\]](#)
28. Stewart, G.M.; Robertson, A.; Jonkman, J.; Lackner, M.A. The creation of a comprehensive metocean data set for offshore wind turbine simulations. *Wind Energy* **2016**, *19*, 1151–1159. [\[CrossRef\]](#)
29. El Beshbichi, O.; Rødstøl, H.; Xing, Y.; Ong, M.C. Prediction of long-term extreme response of two-rotor floating wind turbine concept using the modified environmental contour method. *Renew. Energy* **2022**, *189*, 1133–1144. [\[CrossRef\]](#)
30. Rivera-Arreba, I.; Li, Z.; Yang, X.; Bachynski-Polić, E.E. Comparison of the dynamic wake meandering model against large eddy simulation for horizontal and vertical steering of wind turbine wakes. *Renew. Energy* **2024**, *221*, 119807. [\[CrossRef\]](#)

Disclaimer/Publisher’s Note: The statements, opinions and data contained in all publications are solely those of the individual author(s) and contributor(s) and not of MDPI and/or the editor(s). MDPI and/or the editor(s) disclaim responsibility for any injury to people or property resulting from any ideas, methods, instructions or products referred to in the content.